Journal of Neuroscience Methods 171 (2008) 165–173

Contents lists available at ScienceDirect

Journal of Neuroscience Methods

journal homepage: www.elsevier.com/locate/jneumeth

Semi-automated quantification of filopodial dynamics

Santiago Costantino[a,b,c,*], Christopher B. Kent[b], Antoine G. Godin[a], Timothy E. Kennedy[b], Paul W. Wiseman[a,d], Alyson E. Fournier[b]

[a] Department of Physics, McGill University, Montreal, Canada
[b] Montreal Neurological Institute, Department of Neurology and Neurosurgery, McGill University, Montreal, Canada
[c] Maisonneuve-Rosemont Hospital and Department of Ophthalmology, University of Montreal, Montreal, Canada
[d] Department of Chemistry, McGill University, Montreal, Canada

ARTICLE INFO

Article history:
Received 13 August 2007
Received in revised form 11 February 2008
Accepted 12 February 2008

Keywords:
Growth cone dynamics
Filopodia dynamics
Single particle tracking
Filopodia tracking
Automated quantification fluorescence microscopy
Image analysis

ABSTRACT

Cellular motility underlies critical physiological processes including embryogenesis, metastasis and wound healing. Nerve cells undergo cellular migration during development and also extend neuronal processes for long distances through a complex microenvironment to appropriately wire the nervous system. The growth cone is a highly dynamic structure that responds to extracellular cues by extending and retracting filopodia and lamellipodia to explore the microenvironment and to dictate the path and speed of process extension. Neuronal responses to a myriad of guidance cues have been studied biochemically, however, these approaches fail to capture critical spatio-temporal elements of growth cone dynamics. Live imaging of growth cones in culture has emerged as a powerful tool to study growth cone responses to guidance cues but the dynamic nature of the growth cone requires careful quantitative analysis. Space time kymographs have been developed as a tool to quantify lamellipodia dynamics in a semi-automated fashion but no such tools exist to analyze filopodial dynamics. In this work we present an algorithm to quantify filopodial dynamics from cultured neurons imaged by time-lapse fluorescence microscopy. The method is based on locating the end tips of filopodia and tracking their locations as if they were free-moving particles. The algorithm is a useful tool and should be broadly applicable to filopodial tracking from multiple cell types.

1. Introduction

Appropriate neuronal extension and guidance is critical to attain reliable wiring of the nervous system during development. A myriad of guidance cues including netrins, semaphorins, slits and ephrins bind to specific receptors on the growth cone surface and initiate signals to remodel the growth cone cytoskeleton (Huber et al., 2003; Luo, 2002). How the growth cone interprets multiple cues in time and space to regulate directional motility has only been partially elucidated. This motility is ultimately regulated by a complex interplay of polymerization and disassembly of the actin and microtubule cytoskeleton and the extension of the plasma membrane via vesicle fusion (Bray and Hollenbeck, 1988). Actin filaments underlie lamellipodia and filopodia in the highly dynamic peripheral region of the growth cone and the organization of actin filaments is different in these two structures (Bray and Chapman, 1985). While actin filaments within filopodia are bundled and linear, filaments form a meshwork within the lamellipodial veil (Kalil and Dent, 2005; Mongiu et al., 2007). It has long been appreciated that filopodia and lamellipodia subserve distinct functions highlighting the need to study the dynamics of these structures independently (Albrecht-Buehler, 1976).

Careful quantification of growth cone dynamics is a requirement for the development of a statistically relevant understanding of fine aspects of neuronal motility. The tools to quantify this motility from time-lapse images of dynamic growth cones are in constant development, but a method to precisely assess filopodial dynamics is still lacking and must be performed manually. Systematic studies of lamellipodial behavior has been achieved by using kymograph analysis (Mongiu et al., 2007) and in studies examining growth cones guided by laser light (Betz et al., 2007). Neurite-tracing algorithms varying in complexity and accessibility have also been developed over many years (Capowski, 1989) to trace long extensions such as axons and dendrites. Most available procedures need human interaction, but significant progress in levels of accuracy and automation has been achieved (Al-Kofahi et al., 2002; He et al., 2003; Meijering et al., 2004; Zhang et al., 2007). Comparatively, examination of filopodial dynamics has relied on manual tracking of individual filopodia; a prohibitively time-consuming approach for large-scale analysis. Some recent studies include quantitative

* Corresponding author at: Hôpital Maisonneuve-Rosemont, 5415 boulevard de L'Assomption, Montréal, Que., Canada H1T 2M4 .
Tel.: +1 514 398 1687/252 3400x4958; fax: +1 514 398 8434/251 7094.
E-mail address: santiago.costantino@umontreal.ca (S. Costantino).

0165-0270/$ – see front matter © 2008 Elsevier B.V. All rights reserved.
doi:10.1016/j.jneumeth.2008.02.009

analysis of motility and neurite extension rates (Endo et al., 2003, 2007) but these studies consider the movement of the growth cone as a whole and changes in filopodial extension are considered over long-time scales by manual analysis.

Here we describe a semi-automated method to measure filopodia length and extension and retraction rates from time-lapse images of fluorescently labeled growth cones. We combine simple tracing algorithms and standard single particle-tracking techniques to achieve the first method to accurately quantify filopodial dynamics to the best of our knowledge. We describe the fundamental steps of the algorithm based on skeletonization of isolated growth cones to find the position of their filopodial tips followed by tracking of the tips as individual single particles. The full procedure can be implemented by combining publicly available plug-ins and functions, thus the method will be readily available for general use. An implementation programmed in Matlab (MathWorks Inc., Natick, MA) is made available and procedures for implementation in ImageJ (http://rsb.info.nih.gov/ij/index.html) are also outlined. The results obtained on time-lapse fluorescence images of chick dorsal root ganglia (DRG) growth cones are compared with manual tracings yielding no significant difference from a statistical point of view, while shortening the analysis time by several orders of magnitude.

2. Methods

To semi-automate quantification of filopodial dynamics, individual filopodia from fluorescent time-lapse images of growth cones are selected and skeletonized. The skeleton is the minimum amount of information needed to process a pattern and is obtained by sequentially thinning the objects in an image. This thin-line representation of a pattern is more amenable to extraction of critical features such as end points, junction points and connections among components. As expected, for a thinning algorithm to be effective it should preserve significant features of the pattern and eliminate local noise without introducing distortions of its own (Lam et al., 1992). From skeletons, filopodial end points are detected and traced relative to a start point. Coordinates of individual filopodial tips are tracked as individual free particles through an image sequence from a time-lapse movie and rates and lengths of filopodial extensions and retractions can then be derived. The methods for processing the images and deriving this information are described below.

The first step to achieve a reliable thin-line representation of fluorescent growth cone images is to obtain a good transformation of grayscale images to binary images. This can be performed by applying intensity thresholds (Section 2.1) or alternatively, by detecting object boundaries (Section 2.2). In the first case a threshold value is set, so that all pixels with intensities above this threshold are converted to 1 and dimmer pixels are set to 0. Alternatively, the derivative of the intensity can be analyzed to detect the edges of the objects in the image and set the pixels inside the objects to 1 and the pixels outside to 0.

2.1. Intensity-based binarization

2.1.1. Background estimation

To improve the homogeneity of the image illumination and subtract smooth continuous background, morphological operations are performed. These morphological operations can always be mathematically described as combinations of dilations and erosions. Dilation adds pixels to the boundaries of objects in an image, while erosion removes pixels on object boundaries. The number of pixels added or removed from the objects in an image depends on the size and shape of the structuring element used to process the image. After dilation, the value of a pixel is the maximum value of all the pixels in its neighborhood. In a binary image, if any of the pixels is set to the value 1, the output pixel is set to 1. After erosion, the value of a pixel is the minimum value of all the pixels in its neighborhood. In a binary image, if any of the pixels is set to 0, the output pixel is set to 0 (Gonzalez et al., 2004).

The effect of an opening operator is to preserve foreground regions that have a similar shape to the structuring element, or that can completely contain the structuring element, while eliminating all other regions of foreground pixels. This procedure usually helps when the illumination is not even throughout the field of view, or when the background in bright areas is more intense than the fluorescence in the dim regions. The opening operator specifically consists of an erosion followed by a dilation using the same structuring element (Haralick and Shapiro, 1992). A disk larger than the objects that need to be analyzed is used as a structuring element and *imopen* and *strel* Matlab functions are utilized and the final size can be adjusted depending on the size of the image and the growth cones; the same functions are available in ImageJ using *Subtract Background* with a rolling ball algorithm (Sternberg, 1983).

2.1.2. Intensity threshold

A manually chosen factor of the mean image intensity is set as a threshold. Typically, for the time-lapse fluorescence imaging of our test sets, values above the mean are appropriate to achieve binary images that reliably represent the shape of the growth cones. This is due to the high-signal-to-noise ratio of fluorescence intensity obtained in our neuronal cultures, but for weaker signals a more sophisticated way to establish this threshold value may be required. Manual inspection of several thresholded individual single frames throughout the movie avoids artifacts caused by illumination changes and focus corrections. The intensity value calculated using Otsu's method (Otsu, 1979) is used as a default to begin before such inspection.

2.1.3. Growth cone selection

To discard pixels with intensities above the set threshold that do not belong to the growth cone, an eight-connected neighborhood matrix is established to define individual objects. This assigns all pixels touching vertically, horizontally or diagonally to the same object. The surface of all of the objects present in the image is calculated and only the largest object is conserved. In most cases this procedure is sufficient to discard both noise and debris from the primary culture from the analysis. The functions *regionprops* and *Analyze Particles* can be used to achieve this in Matlab and ImageJ, respectively.

2.1.4. Boundary smoothing

Optimal skeletonization of the growth cone is achieved by simplifying the ramifications protruding from the growth cone. This diminishes false positive filopodia generated from small growth cone protrusions. Growth cone simplification is performed through a sequence of morphological operations to smoothen the edges. In some cases smoothing the growth cone may result in the loss of some small real features present in the image; however, tracking of every end point is not necessary to obtain significant data.

First a closing operation with a custom disk is applied to the images and then a dilation of an arbitrary number of pixels is performed. The adjustment of the dilation magnitude is performed to avoid the fusion of individual filopodia. In our samples two pixels were typically used. Operations can be easily performed in both Matlab (*imclose* and *imdilate*) and ImageJ (*dilate* and *close* in the *Binary* menu).

2.2. Edge detection-based binarization

An algorithm based on the derivative of the intensity can be used to detect the edges of the growth cones. Different implementations

of this type of procedure are available with distinct sensitivity to noise, particularly when the image contrast is low.

2.2.1. Boundary estimation

The *zerocross* edge detection function implemented in Matlab yields the most accurate results in order to perform the skeletonization on our growth cone image sets. The zero-crossing detector filters the image with the Laplacian of a two-dimensional Gaussian of a custom radius and searches for the places in an image where it changes sign. Such points often occur at "edges" in images, points where the intensity of the image changes rapidly, but they also might occur at places that are not as easy to associate with edges. To remove these unwanted events, a threshold for the strength of this derivative value can be manually set. Based on the results obtained on our image sets, the high sensitivity to noise of Sobel filters to find the edges was the reason to choose the Laplacian of a Gaussian as the default method. In order to process the computation we used a lower-order method with [1 1 1; 1, −4, 1; 1 1 1] filter. Similar results can be obtained with ImageJ *Find Edges* function.

2.2.2. Growth cone delineation

The pixels obtained as boundaries are usually not all connected. Different features visible in the original images yield individually connected pixels generating multiple objects. A fraction of such individual objects belong to the growth cone and some others are related to culture debris or noise.

In order to connect the distinct objects, a series of morphological operations are performed. A closing operation with a custom size disc followed by a dilation of an arbitrary number of pixels accomplishes the object unification and smoothens the boundaries at the same time. Subsequently, the biggest object in the image is selected and the remainders are discarded before performing the skeletonization: Matlab (*imclose* and *imdilate*) and ImageJ (*dilate* and *close* in the *Binary* menu).

2.3. Skeletonization

Both of the aforementioned procedures (intensity- and edge detection-based binarizations) render a one-object binary image for skeletonization. To obtain a skeleton, iterative algorithms that delete successive layers of pixels on the boundary of the pattern are applied until only a skeleton remains. The deletion or retention of a pixel p would depend on the configuration of pixels in the local neighborhood containing p. We have chosen an algorithm that provides the simplest structures combined with fast computation time and is the second alternative proposed in an article by Guo and Hall, which is implemented in Matlab by the function *bwmorph* with option *thin* (Guo and Hall, 1989; Lam et al., 1992).

The algorithm is fully parallel, very fast and, more importantly, it preserves the connectivity properties of the image. The skeletonization method included in ImageJ is an alternative, but this algorithm usually yields overly intricate objects with multiple ramifications.

2.4. Identification and localization of ends and intersections

The skeleton obtained for each frame of the time series is scanned in order to find ends and joints. To locate the ends, the pixels with only one neighbor are selected. Similarly, to locate intersections three- or four-neighbor pixels are found. Our implementation uses *find_skel_ends* and *find_skel_intersection* available in Matlab Central (http://www.mathworks.com/matlabcentral/).

2.5. Filopodial tips tracking

To measure the filopodia length as a function of time, the ends found in the skeletonization are tracked as if they were individual free particles. In principle, considering these locations as freely moving entities adds degrees of freedom that the system does not have and including constraints to the tracking algorithm should improve the accuracy of the results. Nevertheless, single particle-tracking methods are widely available, tested and implemented in several different languages. We used Blair and Dufresne's code (http://www.seas.harvard.edu/projects/weitzlab/matlab/).

The following parameters are manually set before performing particle tracking to optimize the results: the minimal duration of a trajectory to be considered in the analysis, the maximal displacement per frame, and the number of frames that a particle (a filopodial end) can be lost along the trajectory.

2.6. Filopodia length estimation methods

The two main goals of this method are to achieve an accurate measurement of filopodia length as a function of time and to calculate the rates of filopodial extension and retraction. The exact lengths of filopodia are dependent on the definition of the origin and the tracing method. The definition of the filopodial initiation site is not trivial because of the dynamic nature of the growth cone periphery from which it initiates. Nevertheless, the rates of filopodial extension and retraction are less sensitive to their precise initiation point and the tracing procedures. Three alternative definitions of filopodial lengths and initiation sites are tested and compared in this article: manually selected origins, centroid determination and distance along the skeleton.

2.6.1. Manually selected origins

A visual inspection of several frames in the movie, allows the user to set arbitrary locations for the origin of the tracked filopodia. The distance from these locations to the ends are a good measurement of the real filopodial length. Since the filopodia ends are numbered in the output movies of our implementation, the user is able to specifically select the extensions to be processed.

2.6.2. Centroid determination

The simplest way to compute rates of filopodial extension and retraction is to define the distance between the image intensity centroid and each filopodial tip. Using this paradigm the absolute length of each filopodia is overestimated because the initiation point is within the central domain of the growth cone rather than at the growth cone periphery. However, in terms of assessing rates of extension and retraction, there is no significant difference to setting their origin locations based on the morphology of the filopodia.

The growth cone intensity centroid is calculated for each frame using the binary mask created before the skeletonization. Thus, only the intensity of the pixels used to calculate the skeleton is considered in the computation of the centroid location and no external object can bias the result. The formula used to establish the centroid coordinates is:

$$\langle \vec{r} \rangle = \frac{\sum_{\text{skeleton}} \vec{r} I_{i,j}}{\sum_{\text{skeleton}} I_{i,j}}$$

where $\vec{r}$ is the position in i and j pixel coordinates, $I_{i,j}$ is the pixel intensity and the sum is calculated over all the pixels that belong to the growth cone mask.

This approach is advantageous because of its automatic nature and because an overall displacement of the growth cone will be reflected in the position of the centroid. The manually selected origins approach assumes that the movement of the whole growth cone is negligible compared with the changes in the filopodia lengths. In most of the cases we analyzed, this effect did not influence the results, but this could introduce an artifact in long-term studies.

2.6.3. Distance along the skeleton

A more sophisticated and desirable measure of the filopodial length is to follow the skeleton from the end to an arbitrary, user-defined origin location. This option considers the curvature of the filopodial projections when measuring their length. This option is more complicated to implement as an imaging processing software macro and it is computationally more time consuming. Given the very complex ramifications that skeletonizations can yield, graph theory (Wilson, 1996) is used to calculate the path length from the end to the origin of filopodia. All of the pixels in the skeleton are considered vertexes of a graph and their connectivity is established by calculating the distance between all possible pixel pairs. The result is a connectivity matrix C where the C_{ij} elements are 1 if pixels i and j of the skeleton are connected and 0 if they are not.

Arbitrary locations are set as approximate filopodial origins and in each image the closest pixels in the skeleton to these locations are found. Next, to choose the path from a filopodial tip to the origin pixel in the skeleton, the shortest path is calculated using the Floyd–Warshall algorithm. This algorithm calculates the shortest path in a weighted, directed graph in a single execution between all pairs of vertices (Floyd, 1962; Warshall, 1962), considering the distances between two connected pixels as weights. We have used an implementation available in the Graph Theory Toolbox from Matlab Central for this application.

3. Culture and imaging

Fluorescence intensity-based imaging of live growth cones was achieved by culturing dorsal root ganglion explants as previously described (Hsieh et al., 2006). Briefly, explants are dissected from E13 chicks and cultured in growth media (F-12 supplemented with 10% Fetal Bovine Serum and 50 ng/μl of 7S nerve growth factor) on glass-bottomed culture dishes (MatTek Co., Ashland, MA) coated with poly-L-lysine and 20 μg/ml laminin. Recombinant herpes simplex virus (HSV) expressing red fluorescent protein (RFP) was generated using 5*dl*1.2 helper virus and the 2-2 cell line as previously reported (Hsieh et al., 2006). Explants were infected at the time of plating and growth cones positive for red fluorescence were imaged approximately 20 h after time of infection.

Standard epifluorescence microscopy was performed using a 100× 1.3 NA objective and immersion oil on an Axiovert 200M inverted fluorescence microscope (Carl Zeiss Canada, Toronto, ON). 500 ms exposure 8-bit grayscale images were obtained with Northern Eclipse software (Empix Imaging, Mississauga, ON) and a Retiga EXi CCD camera (QImaging, Burnaby, BC) every 2.375 s. Imaging was performed using a climate-controlled stage and chamber which maintained temperature at 37 °C and atmospheric CO_2 at 5%. Images were captured without further pre-processing. Comparison of DIC images and fluorescent images revealed that the fluorescence signal reliably detects filopodial lengths and does not expose aberrant pixels from non-focal plane glare (data not shown). Adaptation of this method for cultures that may be labeled with less robust fluorophores or markers may require further image pre-processing or acquisition with a confocal microscope.

4. Results and discussion

Examples of the sequential operations to locate the filopodial ends using intensity threshold- (Section 2.1) or edge detection- (Section 2.2) based proposed methodologies to obtain binary images are presented in Figs. 1 and 2, respectively. The original fluorescence images of a representative E13 chick dorsal root ganglion growth cone (Fig. 1A) were subjected to background correction operations and then thresholded by a factor of the mean pixel intensity. This value was selected after visually inspecting the binary images resulting from a number of frames (approximately 10 frames per image sequence) and adjusting the intensity threshold to correspond to the one yielding the most accurate representation of the growth cone. Thresholding yielded binary images containing several objects composed of connected pixels (Fig. 1B) and by including only the largest of these objects in subsequent analysis one is left with a binary image which accurately corresponds with the shape of the original growth cone and excludes pixels resulting from culture debris or background fluorescence (Fig. 1C). Alternatively, fluorescent images of the same growth cone (Fig. 2A) were subjected to an edge detection function which defines the contours of the growth cone as well as areas of pixel intensity resulting from culture debris. The resulting image (Fig. 2B) shows the effectiveness of such a function which yields well-defined but somewhat disconnected contours. To more accurately characterize the pattern of filopodia and the shape of the growth cone, a closing operation was performed with a user-defined disk size which connects contours into larger objects and results in a more precise representation of the growth cone shape (Fig. 2C) reconnecting filopodia that otherwise would be lost when the largest object is selected (Fig. 2D). The complexity of growth cone morphologies, even in binary images, presents a significant challenge to generating reliable and accurate skeletons. Binary images from both algorithms were dilated by a user-defined number of pixels which smoothened edge effects (Fig. 1D and E). This resulted in reduced complexity while maintaining the representation of gross morphology and allowing for identification of the endpoints of relevant filopodia. Overall, skeletonization using either algorithms (Figs. 1F and 2F) yields reliable and accurate localizations of the filopodia tips. The most appropriate method can be chosen based on a visual inspection of a number of frames in the movie to analyze. The result will typically depend on the signal-to-background ratio of the fluorescence images and their contrast.

Skeletons obtained using the edge-based algorithm (Fig. 2) are generally more accurate for localization of filopodial tips. Nevertheless, in some cases, gaps in the delineation of long protrusions may cause the loss of filopodia for the analysis or yield artifacts like very fast retraction velocities due to an underestimation of their length in isolated frames. Increasing the size of the structuring disc of the closing operation or the number of dilation pixels can fix the gap, but sometimes at the cost of losing accuracy tracing other filopodia or adding debris in the culture to the growth cone pixels. Conversely, the intensity threshold method provides representative skeletons when the image contrast is high (Fig. 1). However, when lamellipodia are too bright compared to filopodia there can be a tradeoff between loosing short protrusions and capturing long and dimmer filopodia.

The example analyzed in Figs. 1 and 2 shows that both methods can precisely locate the filopodial tips, nevertheless the final structure of the growth cone skeleton may differ. Thus, different full length values of the filopodia can be obtained when estimating them using the traces yielded by the skeletons, but the dynamics are less affected by this, as can be seen in Table 1.

In the case of low signal to background images, preprocessing in the spatial or in the frequency domain may be required to obtain accurate quantification of the growth cone dynamics using this method. In addition to the routine to improve the illumination homogeneity that has already been described, a number of operations on the image intensity histograms can be performed before the analysis. As an example, several approaches can be followed to obtain a reliable skeletonization by enhancing the image contrast. The simplest possibility is to remap the image histogram so that a low percentage of the pixels will be saturated at low and high intensities. Alternatively, the grayscale image histogram can be remapped to an arbitrary shape by histogram equalization. This is a technique that aims to modify the dynamic range of the image

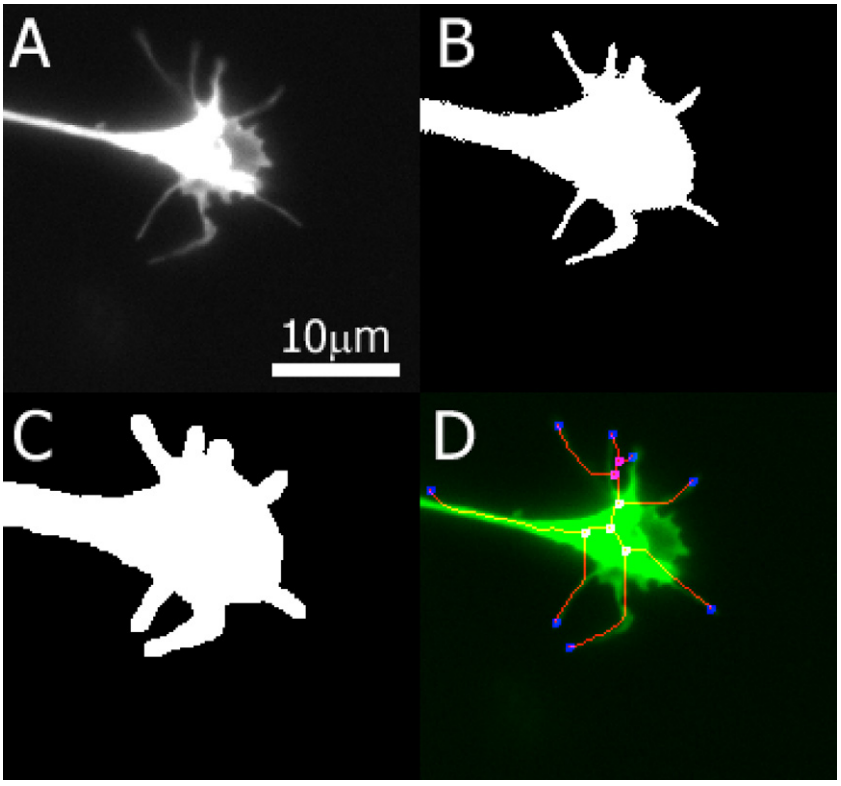

Fig. 1. The sequence of the skeletonization algorithm based on an intensity threshold. (A) The original epifluorescence image. (B) The binary image after applying an intensity threshold. (C) The object is dilated a custom number of pixels to simplify the skeleton and a closing morphological operation is performed with a disk to smoothen the edges. (D) The skeleton obtained is superimposed over the image. The skeleton ends and intersections are labeled with blue and pink circles, respectively. (For interpretation of the references to color in this figure legend, the reader is referred to the web version of the article.)

intensity, in the sense that more frequent pixels should be entitled to a larger range and gain contrast. While this method will typically enhance some regions of the image, it will also result in overexposures of several other areas of the image. Finally, this method is usually applied to spatially independent regions of the image in the so-called contrast-limited adaptive histogram equalization algorithms (CLAHE). CLAHE operates on small regions in the image, called tiles, rather than the entire image. Each tile's contrast is enhanced, so that the histogram of the output region approximately matches a specified histogram. The neighboring tiles are

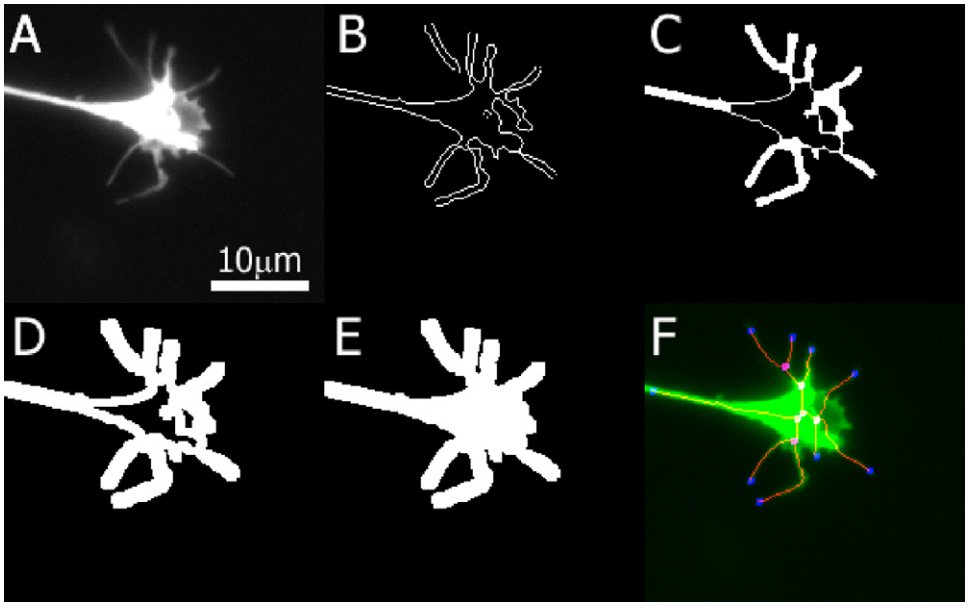

Fig. 2. The sequence of the skeletonization algorithm based on the detection of the edges. (A) The image before image processing. (B) A *zerocross* edge detection operation is performed in order to reveal the contour of the growth cone. (C) A closing operation is done to join filopodia that may be disconnected to the big object. (D) The biggest object of the image is selected given an eight-connectivity matrix. (E) A dilation of a custom number of pixels aids to simplify the skeletonization, by reducing the branching complexity. (F) The skeleton obtained is superimposed over the fluorescence image. The skeleton ends and intersections are labeled with blue and pink circles, respectively. (For interpretation of the references to color in this figure legend, the reader is referred to the web version of the article.)

Table 1
Comparison of the results obtained using intensity- or edge-based methods to manual tracing

	Intensity-based			Edge-based		
	Arbitrary	Centroid	Follow	Arbitrary	Centroid	Follow
Length	0.8 ± 0.2 (0.9 ± 0.1)	0.9 ± 0.2 (0.9 ± 0.1)	1.7 ± 1.4 (1.0 ± 0.1)	0.8 ± 0.1 (0.9 ± 0.1)	0.8 ± 0.1 (0.9 ± 0.1)	1.6 ± 1.2 (1.1 ± 0.1)
Velocity	0.8 ± 0.2 (0.9 ± 0.1)	0.8 ± 0.2 (0.9 ± 0.1)	2.3 ± 2.3 (1.0 ± 0.1)	0.9 ± 0.1 (0.9 ± 0.1)	0.9 ± 0.1 (0.8 ± 0.1)	2.9 ± 1.7 (1.0 ± 0.1)

then combined using bilinear interpolation to eliminate artificially induced boundaries (Gonzalez et al., 2004).

In the case of light-guided growth cones (Betz et al., 2003; Ehrlicher et al., 2002), a bright laser spot can appear in the fluorescence channels and saturate the image or portions of the filopodia to be tracked. A similar artifact can also be produced by culture debris masking a fraction of the growth cone. In both cases, the delineation of the growth cone will not be adequate, however the dynamics obtained after tracking the filopodia that are clearly visible and not masked will not be affected by an overall misleading delineation.

Tracking algorithms are often utilized to trace the trajectories of single molecules and colloids (Murray and Grier, 1996; Saxton and Jacobson, 1997), but our results demonstrate that they are perfectly applicable for other types of movements. The basis of single particle tracking is to match the positions of particles in subsequent frames by minimizing the overall movement of all the particles tracked in an image (Crocker and Grier, 1996; Sage et al., 2005; Sbalzarini and Koumoutsakos, 2005). When the number of particles to track is very large, more sophisticated algorithms have to be implemented, as in Fluorescence Speckle Microscopy (Ponti et al., 2004; Vallotton et al., 2004) and simple routines are not applicable. Most of the simple methods not only track the particle positions, but also include routines in order to locate them, based on their brightness and shape. In our case, finding the positions to be tracked is achieved by scanning the skeletons and not analyzing the images as these methods do. To do this, several different freely available ImageJ plug-ins exist, as well as routines in Matlab, LabVIEW and IDL, which makes them easy to apply.

Filopodia bifurcation, movements out of the focal plane or excessively rapid displacements may cause the tracking algorithm to separate two trajectories that belong to what appears to be one. Likewise, crossovers of two filopodia can render mislabeled trajectories. While the contribution of such artifacts to the final statistical analysis may be negligible if a large number of filopodia are tracked, deletion of incorrect tracks by manual visual inspection will provide the most reliable analysis. In order to aid this analysis, the algorithm implementation we provide imprints a number identifying each filopodium so that tracking data can be manually corrected (Fig. 3).

To establish the accuracy of our method, fluorescently labeled growth cone filopodia (Fig. 3A) were manually traced using NeuronJ (Meijering et al., 2004) in individual frames (purple lines in Fig. 3B). Similar analysis was performed for each frame from the time-lapse movie and individual filopodia were matched in each frame by visual inspection. For comparison, all filopodial endpoints were determined automatically using the edge detection-based skeletonization method and endpoints were tracked using the software (see Section 2.5). All of the endpoints were traced throughout the movie and the final traces from 180 frames are overlaid on the growth cone from the starting frame (Fig. 3C). Filopodial length measurements for each frame were then made using three different

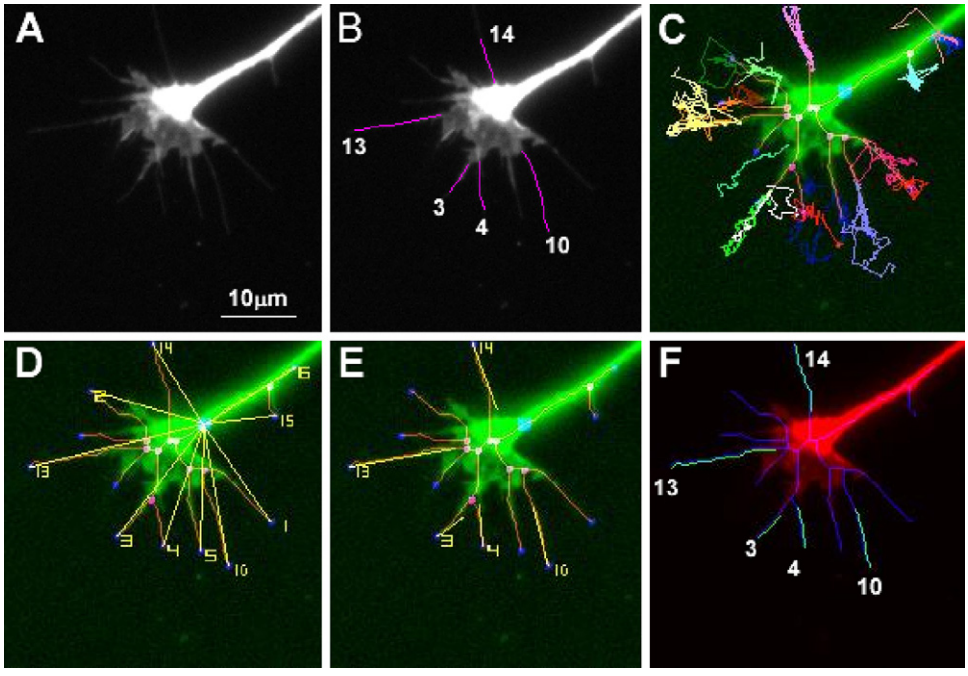

Fig. 3. Depiction of different ways of measuring filopodial dynamics. (A) One frame of the original time-lapse fluorescence images obtained. (B) Selected filopodia were manually traced using NeuronJ (Meijering et al., 2004). This semi-automatic process needs to be repeated for all single frames of the movie. (C) The same particular frame is superimposed with all the trajectories for the whole movie tracked, overlaid and labeled in different colors. (D) For each trajectory, segments from the intensity centroid of the image to the tracked filopodia tips are drawn. All the trajectories are analyzed and numerical labels are automatically added for identification. (E) Manually selecting origin locations in one frame for chosen filopodia, the whole movie was reanalyzed and a more accurate estimation of the absolute length was obtained. (F) The closest skeleton pixels to the same origin points selected before are found. Next, the distance from the filopodia end to these pixels is calculated along the skeleton. (For interpretation of the references to color in this figure legend, the reader is referred to the web version of the article.)

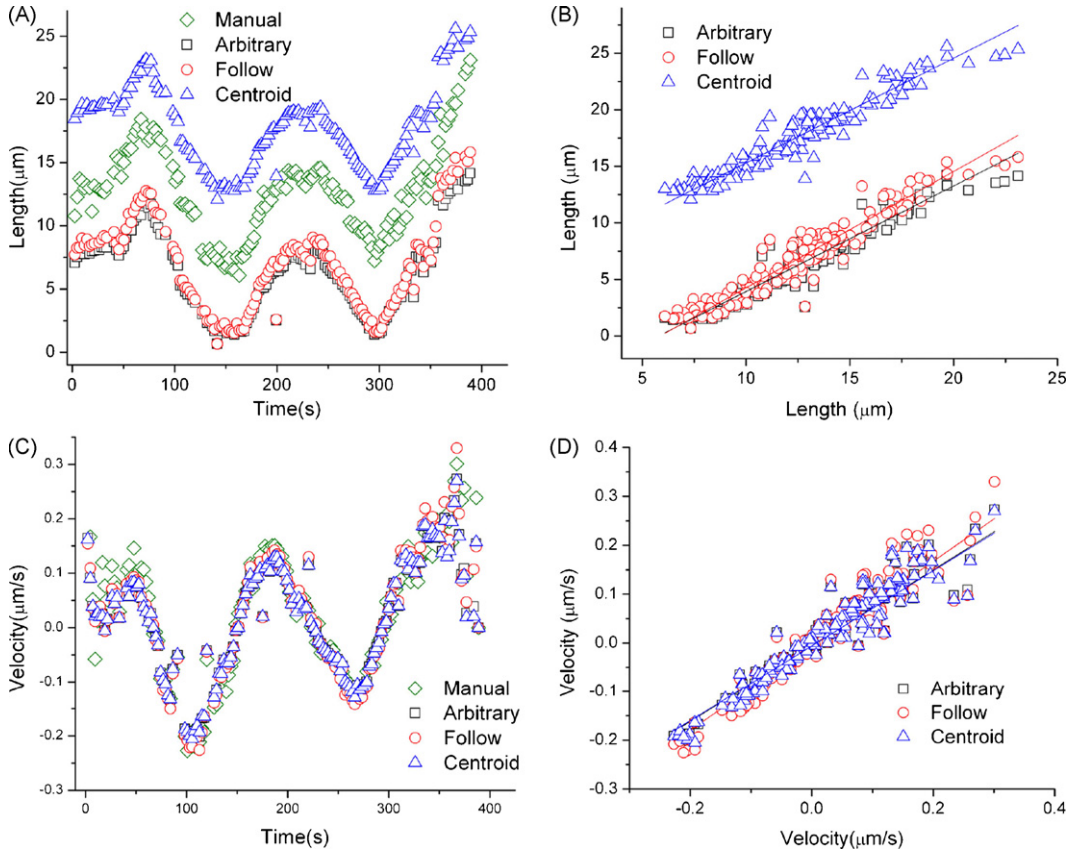

Fig. 4. Comparison of filopodial dynamics quantification from a single manual filopodial tracing vs. methods from the semi-automated algorithm. (A) The lengths obtained in each frame are shown when proceeding manually (green diamonds), the distance calculated from the growth cone centroid (blue triangles), length from manually chosen locations (black squares) and the measure along the filopodia (red circles). (B) The lengths obtained with the algorithms are plotted as a function of the ones manually measured and linear regressions are calculated. (C) The velocity of the filopodia was calculated and plotted for the different methods after smoothing the traces in A. (D) Linear regressions are also performed to compare the velocity values obtained with the algorithm. (For interpretation of the references to color in this figure legend, the reader is referred to the web version of the article.)

methods: centroid determination (yellow bars, Fig. 3D), manually selected origins (yellow bars, Fig. 3E) and distance along the skeleton (white lines Fig. 3F). Panels 3D–F illustrate length measurements from the 77th frame of the movie.

The absolute lengths obtained using the different methods (Fig. 4A) and the extension and retraction rates calculated from these measurements (Fig. 4C) are compared to the numbers obtained from the manual tracings, providing strong confirmation that our software provides filopodial dynamic data which is as accurate as manual tracing. Differences in the absolute length values can be noticed in Fig. 4A because of the rules used to define the filopodial initiation point and need to be taken into account if absolute values of filopodial lengths are of interest. The same arbitrary locations chosen for filopodia are used for the *Follow* and *Arbitrary* methods, in *Manual* tracings the origin and endpoint are relocalized in all frames and in *Centroid* there is a unique origin for all the filopodia in every frame rendering always longer lengths. When there is a global shift of the growth cone, a systematic difference between the methods that use fixed stationary coordinates and the ones that update them in every frame will arise.

The correlation between the length obtained using each method and the length determined by manual tracing was calculated by performing two-dimensional linear regressions. For the five filopodia that were manually tracked, we plotted the length obtained with the different algorithms as a function of the value measured manually for all the frames in the movie. A linear regression was performed for all of the manually traced filopodia and the mean slopes obtained with each method are shown in Table 1 where standard deviation values are shown as absolute errors. The accuracy of the method can be demonstrated by comparing the values obtained manually and using the algorithms. The linear regression of the computed lengths and velocities as a function of the values obtained manually should yield a slope of 1 and a minimal dispersion around a straight line. The magnitude of the slope reflects the accuracy of the method, while the error of the linear fit reflects the precision. In addition, we calculated the probability p-values for testing the hypothesis of no correlation. Each p-value is the probability of having a correlation as large as the observed value by random chance, when the true correlation is zero, yielding always less than 5%. An example of this correlation is shown in Fig. 4B for the trajectory obtained for filopodia number 10 (Fig. 3D) and its dynamics in Fig. 4D.

The values obtained for the methods that consider filopodia as straight lines show small, systematic differences compared to manual tracing. The reason for this is that even if both origin and end point of filopodia coincide, the curved trace will always result in a longer length. Furthermore, the magnitude of this difference will increase with the total length of the filopodium.

The results achieved for the length and velocity determined by following the skeleton show the converse effect. Since the skeleton changes in the lamellipodial region, in some frames the closet pixel to the one manually defined belongs to another filopodia and this produces jumps between skeleton branches causing overestimations of the length which are reflected in the high correlation slopes. When this happens, it is necessary to visually identify the filopodia that produce these artifacts and remove them from the

analysis. The results taking into account only four filopodia instead of five are shown in parentheses (Table 1).

To our knowledge the method presented here is the first method described to quantify filopodial dynamics from time-lapse-imaging sequences thus the results of our routine can only be compared to results achieved with manual tracings in individual frames. Other neurite-tracing algorithms lack the sensitivity or automation of this routine. This filopodial-tracing routine allows for an automated or semi-automated selection of a single filopodium in the first frame of a time-lapse image sequence and subsequent automated tracking of a filopodium through a stack of time-lapse images. Freely available software such as the NeuronJ plug-in for ImageJ requires manual selection of initiation and end points for individual neurites and would thus require time-consuming analysis of each filopodium in individual frames of the time-lapse movie. More automated neurite-tracing routines such as NeuriteTracer (Pool et al., doi:10.1016/j.jneumeth.2007.08.029) rely on a thresholding paradigm that would fail to distinguish individual filopodia. Skeletonizing a growth cone image using this type of neurite-tracing program would result in a single continuous branched structure including the neurite stalk and all filopodial protrusions with the growth cone reduced to a single pixel. Short filopodia would be lost as they would not be distinguished from the growth cone and individual filopodia would not be distinguished. The irregular shapes of growth cones (compared to relatively round cell bodies) would likely result in false positive filopodial traces. Commercially available neurite-tracing programs such as MetaXpress (http://www.moleculardevices.com/pages/software/metaxpress.html) would suffer from the same issues as NeuriteTracer. The technique we present combines a simple approach for tracing individual filopodia, with a solution to find and match filopodial tips in subsequent images, providing a useful tool to quantify this dynamic process.

5. Conclusions

The method we introduce provides a tool to quantify and automate the analysis of filopodial dynamics. We have shown that the algorithm is accurate and opens the door to perform a collection of quantitative measurements including length and protrusion and retraction rates. Furthermore, the automation provided by this method yields a major improvement in the number of filopodia that can be measured compared with manual tracing, providing statistically relevant results. We have demonstrated that the original concept of tracking filopodial end tips as individual single particles allows the quantification of complex dynamic behaviors without the need for further development of temporally based neurite-tracing algorithms.

The formation, extension and retraction of actin-based filopodial structures represent important dynamic processes that regulate cell motility in a wide variety of contexts. The development of this tool will not only be of benefit to the study of filopodial dynamics in neuronal growth cones but also could be applied to quantifying the behavior of similar structures in various motile cell types which underlie critical physiological processes.

The Matlab implementation of our routine is publicly offered as open-source code in the form of individual functions and also with a graphical user interface together with a test data set (http://fournierlab.mcgill.ca). A compiled version is also available by request.

Acknowledgements

This work is supported by a CIHR grant to AEF and by the McGill Program in Neuroengineering. Support is acknowledged for AEF from CIHR, for PWW from NSERC, CIHR and FQRNT, for TEK from FRSQ and CIHR, for SC and AGG from the Neurophysics CIHR Strategic Training Grant and for SC from the McGill Program in NeuroEngineering. We thank S. Iglin (graph theory), A. Fong (find end and intersections), J. Tian (lines drawing), P. Cermelj (ini files handling) for functions downloaded from Matlab Central and D. Balir and Eric Dufresene for the tracking routine.

Appendix A. Supplementary data

Supplementary data associated with this article can be found, in the online version, at doi:10.1016/j.jneumeth.2008.02.009.

References

Al-Kofahi KA, Lasek S, Szarowski DH, Pace CJ, Nagy G, Turner JN, et al. Rapid automated three-dimensional tracing of neurons from confocal image stacks. IEEE Trans Inf Technol Biomed 2002;6:171–87.
Albrecht-Buehler G. Filopodia of spreading 3T3 cells. Do they have a substrate-exploring function? J Cell Biol 1976;69:275–86.
Betz T, Ehrlicher A, Stuhrmann B, Koch D, Schreck F, Moore S, et al. Guiding neuronal growth with light. Biophys J 2003;84, 416a–416a.
Betz T, Koch D, Stuhrmann B, Ehrlicher A, Kas J. Statistical analysis of neuronal growth: edge dynamics and the effect of a focused laser on growth cone motility. New J Phys 2007;9:426.
Bray D, Chapman K. Analysis of microspike movements on the neuronal growth cone. J Neurosci 1985;5:3204–13.
Bray D, Hollenbeck PJ. Growth cone motility and guidance. Annu Rev Cell Biol 1988;4:43–61.
Capowski JJ. Computer techniques in neuroanatomy. New York: Plenum Press; 1989.
Crocker JC, Grier DG. Methods of digital video microscopy for colloidal studies. J Colloid Interf Sci 1996;179:298–310.
Ehrlicher A, Betz T, Stuhrmann B, Koch D, Milner V, Raizen MG, et al. Guiding neuronal growth with light. Proc Natl Acad Sci USA 2002;99:16024–8.
Endo M, Ohashi K, Mizuno K, Kinase LIM. Slingshot are critical for neurite extension. J Biol Chem 2007;282:13692–702.
Endo M, Ohashi K, Sasaki Y, Goshima Y, Niwa R, Uemura T, et al. Control of growth cone motility and morphology by LIM kinase and slingshot via phosphorylation and dephosphorylation of cofilin. J Neurosci 2003;23:2527–37.
Floyd R. Algorithm 97: shortest path. Commun ACM, 1962;5:345.
Gonzalez RC, Woods RE, Eddins SL. Digital image processing using MATLAB. Upper Saddle River, NJ: Pearson Prentice Hall; 2004.
Guo Z, Hall RW. Parallel thinning with 2-subiteration algorithms. Commun ACM 1989;32:359–73.
Haralick RM, Shapiro LG. Computer and robot vision. Reading, MA: Addison–Wesley Publishing Co; 1992.
He W, Hamilton TA, Cohen AR, Holmes TJ, Pace C, Szarowski DH, et al. Automated three-dimensional tracing of neurons in confocal and brightfield images. Microsc Microanal 2003;9:296–310.
Hsieh SH, Ferraro GB, Fournier AE. Myelin-associated inhibitors regulate cofilin phosphorylation and neuronal inhibition through LIM kinase and slingshot phosphatase. J Neurosci 2006;26:1006–15.
Huber AB, Kolodkin AL, Ginty DD, Cloutier JF. Signaling at the growth cone: ligand–receptor complexes and the control of axon growth and guidance. Annu Rev Neurosci 2003;26:509–63.
Kalil K, Dent EW. Touch and go: guidance cues signal to the growth cone cytoskeleton. Curr Opin Neurobiol 2005;15:521–6.
Lam L, Lee SW, Suen CY. Thinning methodologies—a comprehensive survey. IEEE Trans Pattern Anal Mach Intell 1992;14:869–85.
Luo LQ. Actin cytoskeleton regulation in neuronal morphogenesis and structural plasticity. Annu Rev Cell Dev 2002;18:601–35.
Meijering E, Jacob M, Sarria JC, Steiner P, Hirling H, Unser M. Design and validation of a tool for neurite tracing and analysis in fluorescence microscopy images. Cytometry A 2004;58:167–76.
Mongiu AK, Weitzke EL, Chaga OY, Borisy GG. Kinetic-structural analysis of neuronal growth cone veil motility. J Cell Sci 2007;120:1113–25.
Murray CA, Grier DG. Video microscopy of monodisperse colloidal systems. Annu Rev Phys Chem 1996;47:421–62.
Otsu N. Threshold selection method from gray-level histograms. IEEE Trans Syst Man Cybern 1979;9:62–6.
Ponti A, Machacek M, Gupton SL, Waterman-Storer CM, Danuser G. Two distinct actin networks drive the protrusion of migrating cells. Science 2004;305:1782–6.
Sage D, Neumann FR, Hediger F, Gasser SM, Unser M. Automatic tracking of individual fluorescence particles: application to the study of chromosome dynamics. IEEE Trans Image Process 2005;14:1372–83.
Saxton MJ, Jacobson K. Single-particle tracking: applications to membrane dynamics. Annu Rev Biophys Biomol Struct 1997;26:373–99.
Sbalzarini IF, Koumoutsakos P. Feature point tracking and trajectory analysis for video imaging in cell biology. J Struct Biol 2005;151:182–95.

Sternberg SR. Biomedical image-processing. Computer 1983;16:22–34.
Vallotton P, Gupton SL, Waterman-Storer CM, Danuser G. Simultaneous mapping of filamentous actin flow and turnover in migrating cells by quantitative fluorescent speckle microscopy. Proc Natl Acad Sci USA 2004;101:9660–5.
Warshall S. A theorem on Boolean matrices. Commun ACM 1962;9:11–2.
Wilson RJ. Introduction to graph theory. Addison–Wesley; 1996.
Zhang Y, Zhou X, Degterev A, Lipinski M, Adjeroh D, Yuan J, et al. A novel tracing algorithm for high throughput imaging screening of neuron-based assays. J Neurosci Methods 2007;160:149–62.